Significant Reduction in Thermal Conductivity of Lithium Cobalt Oxide Cathode Upon Charging: Propagating and Non-propagating Thermal Energy Transport

Shiqian Hu,[1,2,3] Zhongwei Zhang,[1,2,3] Zhongting Wang,[4] Kaiyang Zeng,[4] Yuan Cheng,[5] Jie Chen,[1,2,3,*] and Gang Zhang[5*]

There are growing efforts towards the control of thermal transport in the lithium-ion (Li-ion) battery, where thermal conductivity of cathode material is one of the most important material parameters that determine the safety. Despite playing critical role, fundamental understanding of thermal conductivity and how delithiation changes thermal conductivity are still an uncharted territory. To this end, we investigate the effect of delithiation on thermal conductivity of $LiCoO_2$, a common Li-ion cathode material, by using non-equilibrium molecular dynamics simulations and lattice dynamics analysis. A significant reduction (exponential decay behavior) in thermal conductivity is observed in the delithiation (charging) process. For instance, thermal conductivity is only 30% of pristine cathode comparing with 20% of delithiation. The calculation results of heat energy transmission coefficient and spectral energy density together suggest that the delithiation induces ordered-to-disordered transition, which results in the non-propagating heat transport. Furthermore, the propagating phonon modes are strongly scattered by Li-vacancy. These are responsible for the remarkable reduction of thermal conductivity and the weakened temperature-dependence. Our work establishes a fundamental understanding of the thermal energy transport in cathode materials of Li-ion battery, and emphasizes the important role of delithiation effect in the thermal management in electrochemical energy storage devices.

1. Introduction

In recent years, Lithium ion (Li-ion) rechargeable batteries have served as significant power sources for most portable electronics as well as the electric vehicles because of their high energy density and rate capability. Safety is a key aspect for Li-ion batteries.[1] Under ideal operation, the batteries convert the chemical energy to electrical energy with minimal heat. However, in some abusive cases, the chemical energy may directly convert into heat. For example, overcharge can generate huge heat energy within the battery. Although safety control is not determined by one criterion or parameter, thermal conductivity is still one of the most important material parameters that determine the safety of Li-ion batteries,

modules and battery packs.[2] Even under normal operation, charging/discharging circuit will heat up the battery via Joule heating, and this heat is dissipated through the electrode materials in the format of thermal conduction. If the thermal conductivity of electrode material is not sufficiently high, the temperature will continue to rise. Once the temperature is over a critical value, exothermic reaction will begin and the battery itself produces heat, in which high rate reaction will cause temperature rising sharply and rapid disassembly may occur.[3]

Most commercial Li-ion batteries consist of transition metal oxide cathode such as $LiCoO_2$, graphitic carbon as anode and an organic solvent electrolyte. In contrast to the high thermal conductivity of graphite (~thousands $Wm^{-1}K^{-1}$), room temperature thermal conductivity of $LiCoO_2$ is only about 5.4 $Wm^{-1}K^{-1}$.[4-6] Obviously, compared to graphite based anode, low thermal conductivity in $LiCoO_2$ will be the bottleneck in thermal management of Li-ion batteries. Moreover, during the charging cycle, lithium is moved from the cathode, while the dynamic (Li concentration dependent) thermal conductivity of $LiCoO_2$ is still not well understood, which is challenging in experiment. Despite playing critical role in the safety of Li-ion battery, fundamental understanding of how delithiation changes thermal conductivity and temperature dependence are still an uncharted territory.

In recent years, atomistic simulation has played a vital role in the materials design of advanced Li-ion batteries,[7-12] and has successfully predicted the properties and key performance of battery systems. In particular, the predictions of a variety of properties pertinent to Li-ion batteries have been shown to be accurate, such as the energy density, ion diffusion mobility and the charge/discharge voltage profiles.[13-16] However, previously, the major efforts are

[1]*Center for Phononics and Thermal Energy Science, School of Physics Science and Engineering, and Institute for Advanced Study, Tongji University, Shanghai 200092, People's Republic of China*

[2]*China–EU Joint Lab for Nanophononics, School of Physics Science and Engineering, Tongji University, Shanghai 200092, People's Republic of China*

[3]*Shanghai Key Laboratory of Special Artificial Microstructure Materials and Technology, School of Physics Science and Engineering, Tongji University, Shanghai 200092, People's Republic of China*

[4]*Department of Mechanical Engineering, National University of Singapore, 9 Engineering Drive 1, 117576, Singapore*

[5]*Institute of High Performance Computing, Agency for Science, Technology and Research, 1 Fusionopolis Way, Singapore 138632, Singapore*

*E-mail: jie@tongji.edu.cn (J.C.); zhangg@ihpc.a-star.edu.sg (G. Z.)

focused on the electronic, mechanical and morphological properties, while the thermal property of LiCoO$_2$ upon delithiation is still not clear, despite its crucial role in Li battery safety. Although a fully quantum-mechanical treatment (represented by first-principles calculations) of the system is highly desirable, it can only be applied to the system with a small size due to the large computational load. Molecular dynamics (MD) simulation is another powerful tool to handle many-body problems at the atomic level, and its applications have covered a wide range of material properties, such as mechanical and thermal properties.[17-20] It can explore the thermal conductivity without any thermodynamic-limit assumption, and naturally includes full affecting factors in atomistic interactions. In MD simulations, the force on each atom according to the force field controls the dynamic process of the system. Therefore, tremendous efforts have been devoted to developing empirical potential with the sacrifice of exactness.

In this work, using non-equilibrium molecular dynamics simulations (NEMD), we report the Li-ion flowing modulation of the thermal conductivity in LiCoO$_2$ over the range of 19.8 Wm^{-1}K^{-1} to 5.2 Wm^{-1}K^{-1} for the delithiation degree changing from zero to 40%. Based on the heat energy transmission coefficient, the delithiation induces the non-propagating heat transport mechanism is obtained. Moreover, the underlying physical mechanism of the weak temperature-dependence of the thermal conductivity in the delithiated LiCoO$_2$ is uncovered by comparing the spectral energy density between pristine and delithiated LiCoO$_2$. A clear dynamic modulation picture of the thermal conductivity of LiCoO$_2$ by delithiation is obtained in this work.

2. Computational Methods

MD simulations in this paper are performed by using LAMMPS package.[21] The Buckingham potential combining with a long-range Coulombic component was used to describe the potential energy between pairs of ions in each crystalline solid. The Buckingham potential is denoted as,[22]

$$\Phi_{i,j}(r_{ij}) = A_{ij}exp(-r_{ij}/\rho_{ij}) - C_{ij}/r_{ij}^6 \quad (1)$$

where r is the distance between ions i and j, and A_{ij}, ρ_{ij} and C_{ij} are the potential parameters taken from Ref [22]. The time step is set as 0.5 fs. As shown in Fig. 1a, the periodic boundary conditions are used in all directions. The cut-off distance is set as 10 Å for both Coulombic and Buckingham force. Equilibrium MD simulations with the isothermal-isobaric (NPT) ensemble are first performed for 50 ps, during which the whole system has reached thermal equilibration (Fig. 1b) and the stress in the structure has been fully relaxed (Fig. 1c). Then, the NEMD simulations are performed. To establish a temperature gradient, the atoms near two ends (two shadowed regions in Fig. 1a) are coupled with Langevin heat bath[22,23] at low-temperature T_L, and atoms at the center are attached to high-temperature heat bath at T_H. With the periodic boundary condition, this simulation setup can effectively remove the boundary effect.[25,26] The thermal conductivity κ is calculated based on Fourier's Law,

$$\kappa = -\frac{J}{\nabla T} \quad (2)$$

where ∇T and J are, respectively, the temperature gradient and the heat flux. Fig. 1d shows a typical temperature profile of the LiCoO$_2$ at 300 K. The temperature gradient is obtained by the linear fitting to the local temperature at each side, excluding the temperature jumps

closed to the heat baths. In our simulations, after the system reaching the steady state, the cumulative energy ΔE added/subtracted to the heat source/sink region is recorded for 1 ns. By applying the linear fitting to the raw data of the cumulative energy ΔE (shown in Fig. 1e), the energy change per unit time ($\Delta E/\Delta t$) is obtained, which is used to calculate the heat flux $J = \Delta E/(2S\Delta t)$. Here S is the cross area of LiCoO$_2$ defined as the width (W) multiplied by the thickness, and the factor of 2 accounts for the bidirectional heat flow. The size of the simulation domain is fixed as 25 nm, 3 nm and 3 nm along x, y and z direction, respectively. The results presented here are averaged over 3 independent simulations with different initial conditions, and the error bar is obtained from the standard deviation of different runs.
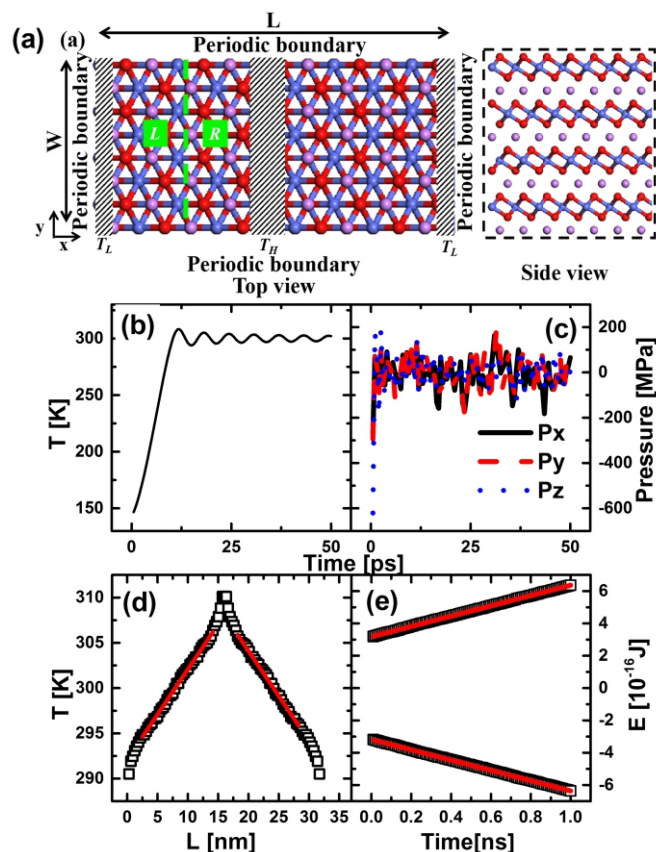

Fig. 1 Simulation setup, structure relaxation, temperature gradient and heat flux calculation. (a) Simulation set up, top view and side view of the LiCoO$_2$. Periodic boundary conditions are used along the length (L) and the width (W) direction. The green dashed line denotes the imaginary plane which divides the system into "L" and "R" two segments. The size of the simulation domain is L= 32 nm and W= 3 nm. (b) The average temperature in the simulation system with the NPT ensemble. (c) The pressure distribution in three directions with the NPT ensemble. (d) The typical temperature profile of the LiCoO$_2$ at 300 K. Linear fitting is performed to obtain the temperature gradient. (e)The typical cumulative energy change in the heat source and heat sink region for the LiCoO$_2$ at 300 K. Linear fitting is performed to obtain the energy change per unit time ($\Delta E/\Delta t$).

3. Results and Discussion

3.1 Rapid reduction in thermal conductivity upon delithiation

The delithiation process in our simulations is realized by randomly removing certain amount of Li-ions in LiCoO$_2$. The delithiation

degree is defined as N_R/N_P, where N_R denotes the number of removed Li-ions and N_P is the total number of Li-ions in pristine $LiCoO_2$. In our simulation, the delithiation degree is varied up to 40%, which is consistent with previous experimental work.[4] As shown in Fig. 2, thermal conductivities of the delithiated $LiCoO_2$ (κ_D) are significantly reduced compared to that of pristine $LiCoO_2$ (κ_P), showing an exponential decay behavior (solid line in Fig. 2) in the delithiation (charging) process. When the delithiation degree increases to 20%, a sharp decrease in κ_D is observed. For instance, κ_D is reduced to 65% of κ_P with only 5% of delithiation, and it is only 30% of κ_P with 20% of delithiation. Further increase of delithiation degree above 20% induces less significant change in κ_D. This behavior is consistent with the previous MD simulations of the defected MoS_2[27] and graphene sheet.[28]
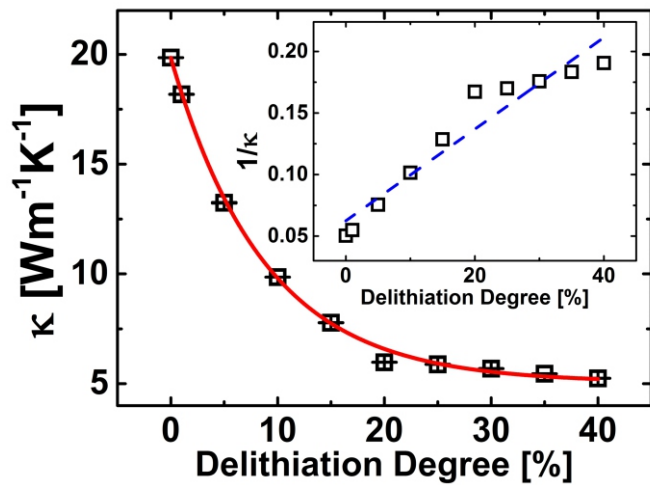
Fig. 2. Thermal conductivity of $LiCoO_2$ changes with the delithiation degree at 300 K. The symbols are numerical simulation results and the solid line is the exponential fitting curve. The insert shows $1/\kappa$ versus the delithiation degree, and the dashed line draws the linear dependence for comparison.

There are Li-vacancies in the delithiated $LiCoO_2$. Phonon scattering by vacancies in crystals is usually treated from perturbation theory in terms of the missing mass and the missing linkages, and the scattering rate is[29]

$$\tau_V^{-1} \sim x\frac{\omega^2 g(\omega)}{N} \tag{3}$$

where x is the density of vacancies, $g(\omega)$ is the phonon density of states, and N is the number of atoms in the crystal. If only considering the Umklapp phonon-phonon scattering (τ_U^{-1}, $\tau_U^{-1} \propto \omega^2$) from the Matthiessen's rule, the total phonon scattering rate τ^{-1} is given as:

$$\tau(\omega)^{-1} = \tau_U^{-1} + \tau_V^{-1} \tag{4}$$

According to the phonon Boltzmann transport equation within relaxation time approximation, the thermal conductivity can be described as:

$$\kappa \sim \int C(\omega)v^2(\omega)\tau(\omega)d\omega \tag{5}$$

where $C(\omega)$ is the heat capacity, $v(\omega)$ is the phonon group velocity vector and $\tau(\omega)$ is the effective phonon relaxation time. Thus we can

have the following relationship:

$$\frac{1}{\kappa} \propto \tau^{-1} \approx A + x \times B \tag{6}$$

where A and B are two constants independent of the density of vacancies.

The insert in Fig. 2 shows $1/\kappa$ as a function of the Li-vacancy concentration x (delithiation degree), which deviates notably from the linear relationship (dashed line in the inset) predicted by Eq. (6). This discrepancy indicates that there might exist other underlying mechanism responsible for the reduction of thermal conductivity. In the following part, we will show that delithiation induced ordered-to-disordered transition plays an important role in this remarkable reduction of thermal conductivity.

### 3.2 Propagating and non-propagating heat energy transport

To shed light on the origin for the reduced thermal conductivity in $LiCoO_2$ after delithiation, we explore the spectral heat energy transmission coefficients in pristine $LiCoO_2$ and the delithiated $LiCoO_2$ with different delithiation degrees following Ref.[30,31] The spectrum distribution of heat energy transmission $T(\omega)$ is calculated as[31]

$$T(\omega) = \frac{q(\omega)}{k_B\Delta T} \tag{7}$$

where k_B is the Boltzmann parameter and ΔT is the temperature difference between the two Langevin thermostats. Here $q(\omega)$ is the frequency dependent heat flux across the imaginary cross-section (green dashed line in Fig. 1a), which can be calculated as:[30,31]

$$q(\omega) = \frac{2}{St_s}Re\sum_{i \in L}\sum_{j \in R}\left\langle \mathbf{F}_{ij}(\omega) \cdot \mathbf{v}_i(\omega)^* \right\rangle \tag{8}$$

where S is the cross area, t_s is the simulation time, and $\mathbf{F}_{ij}$ is the inter-atomic force on atom i due to atom j. Here, "L" and "R" denote the left and right segment, respectively, which are located at two sides of the imaginary cross-section.
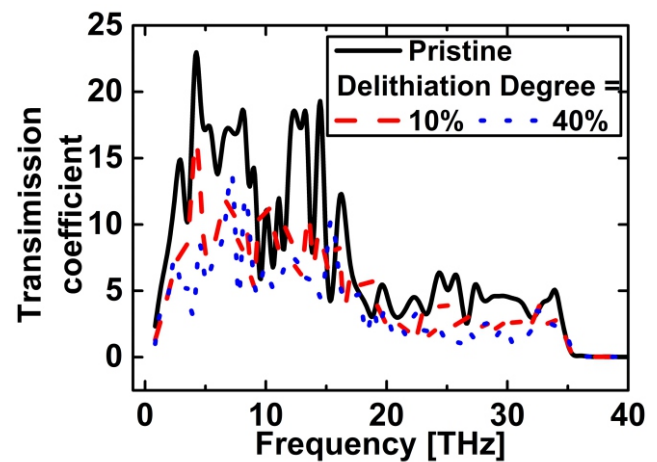
Fig. 3 Heat energy transmission coefficient of the pristine $LiCoO_2$ and delithiated $LiCoO_2$. The heat energy transmission coefficient of pristine $LiCoO_2$ (solid line) and the delithiated $LiCoO_2$ with delithiation degrees as 5% (dashed line) and 10% (dotted line) respectively.

As shown in Fig. 3, we find that after the delithiation process,

the heat energy transmission coefficients in the delithiated $LiCoO_2$ (dashed and dotted line) are significantly suppressed compared to that in pristine $LiCoO_2$ (solid line) for nearly the entire frequency range. For the delithiated $LiCoO_2$, a further decrease is observed when the delithiation degree increases from 10% to 40%. In the phonon-dominated heat transport, low frequency phonons are less sensitive to vacancy[32,33] scattering compared to high frequency phonons, within the frame of perturbation theories by Ratsifaritana and Klemens.[29] Unexpectedly, in $LiCoO_2$, the reduction in heat energy transmission in low frequency regime is even more remarkable than that in the high frequency regime.

In crystals, phonons are the primary carriers of heat energy, which can be described by the kinetic theory such as Boltzmann transport equation.[34] In contrast, in disordered solids, phonons are ill-defined due to the lack of crystalline periodicity, which leads to the loss of definition of the wave vector.[35-39] In 1990s, Allen *et al.*[40] classified the heat carriers in disordered solids as propagons, diffusions, and locons, depending on the degree of localization of each carrier. Simply speaking, propagons are phonon-like carriers in a manner analogous to uncoupled particles, while diffusions carry heat in a random-walk manner. These two are delocalized and the primary heat carriers in disordered solids because locons are localized and nonpropagating.[35] In delithiated $LiCoO_2$, the delithiation disrupts the lattice periodicity, and introduces degree of disorder. Therefore the delithiation of $LiCoO_2$ can give rise to diffusions associated with the phonon-vacancy scattering, and suppress the heat energy transmission in both high and low frequency regimes. As low frequency vibrational modes usually carry more heat energy than high frequency modes, because of the higher density of modes and higher speed of sound, this results in the unexpectedly large reduction in thermal conductivity of $LiCoO_2$ in delithiation process.

3.3 Temperature dependence in thermal conductivity and anharmonic effect

So far, we have investigated the delithiation effect on the thermal transport of the $LiCoO_2$ at 300 K and the underlying mechanism is revealed by analyzing the phonon transmission coefficient. To further study the temperature effects on the thermal transport properties of $LiCoO_2$ and delithiated $LiCoO_2$, we compute the temperature dependence of κ_P and κ_D with different delithiation degrees.

Fig. 4 shows the temperature dependence of the thermal conductivity in pristine $LiCoO_2$ and delithiated $LiCoO_2$. Obviously, all samples exhibit a temperature dependence that does not follow the typical expectation from Debye-Callaway model (T^{-1}), which suggests the presence of a disordering event. The results show that the κ_P and κ_D are decreased at elevated temperature and follow $T^{-\alpha}$ behavior due to the intrinsic Umklapp phonon scattering.[41] And the fitting values of α are 0.53, 0.49, 0.22 and 0.02 corresponding to the pristine and delithiated $LiCoO_2$ with percentage of 5%, 10%, and 40%, respectively. In other words, comparing with the pristine $LiCoO_2$, the thermal conductivity of the delithiated $LiCoO_2$ is less sensitive to the variation of temperature, especially when the delithiation degree is high.

For the pristine $LiCoO_2$, the thermal conductivity follows $T^{-0.53}$ by fitting, which shows a deviation from the Debye-Callaway model (T^{-1}).[42] The possible reason is given as follows. In bulk system, when the phonon-phonon scattering dominates the thermal transport, the
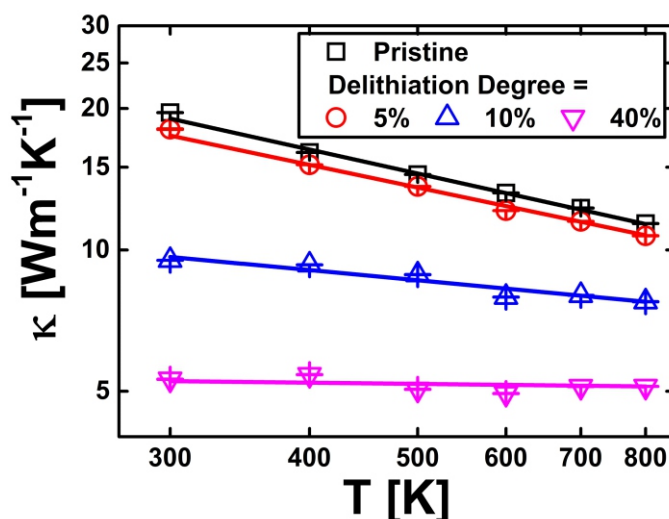
Fig. 4 The temperature effect on the thermal transport properties of $LiCoO_2$ and delithiation $LiCoO_2$. Log-log plot for the temperature dependence of thermal conductivity of $LiCoO_2$ and delithiated $LiCoO_2$ with different delithiation degrees, showing a $T^{-\alpha}$ behavior. The symbols are simulation results and the solid lines are the linear fitting lines. The error bars are standard deviation of 3 independent simulations with different initial conditions.

temperature dependence of the thermal conductivity will follow the Debye-Callaway model,[42] that is, the exponent α equals to 1. However, in our simulations, we fixed the system length L as 32 nm (quite short compared to the phonon mean free path), the boundary scattering should play a significant role in the thermal transport. Our previous work[28] has been verified that the value of α is sensitive to the total length of the simulations domain. And as the length L increases (the boundary effects subside), the value of α will be increased. Hence, for the pristine case, the deviation in α from 1 is due to the boundary scattering causing by the very small system length setting in our simulations.

Anharmonic phonon scattering plays dominated role in temperature dependent thermal conductivity. To understand the underlying physical mechanism for the distinct temperature-dependence of pristine and delithiated $LiCoO_2$, we have calculated the spectral energy density (SED) from atom trajectories, The spectral energy density can be calculated as[43,44]

$$\Phi_{\mathbf{k},p}(\omega) = \frac{1}{4\pi\tau_0 N} \sum_{\alpha}^{3} \sum_{j}^{n} \sum_{l}^{N} m_j \left| \int \dot{u}_\alpha^{l,j}(t) e^{(i\mathbf{k}\cdot\mathbf{r}_0^{l,j} - i\omega t)} dt \right|^2 \qquad (9)$$

where $\mathbf{k}$ is the wave vector, p is the phonon polarization branch, m_j is the atomic mass, N is the total number of unit cells, $\dot{u}_\alpha^{l,j}$ is the velocity of the αth component of the jth atom in the lth unit cell which is dumped from MD simulations, $\mathbf{r}_0^{l,j}$ is the equilibrium position of the atom, and τ_0 is the total integration time. Here, for both pristine and delithiated $LiCoO_2$, the spectral energy density is computed along x-axis direction.

Fig. 5 shows the low frequency part of phonon dispersion curves (< 5THz) in the pristine and delithiated $LiCoO_2$ at 300 K. The shading on the plot indicates the magnitude of the spectral energy density for each phonon mode.[43] And the magnitude increases when the color varies from blue to red. In the pristine $LiCoO_2$ (Fig. 5a), the longitudinal acoustic (LA) branch and two transverse acoustic (TA$_1$,
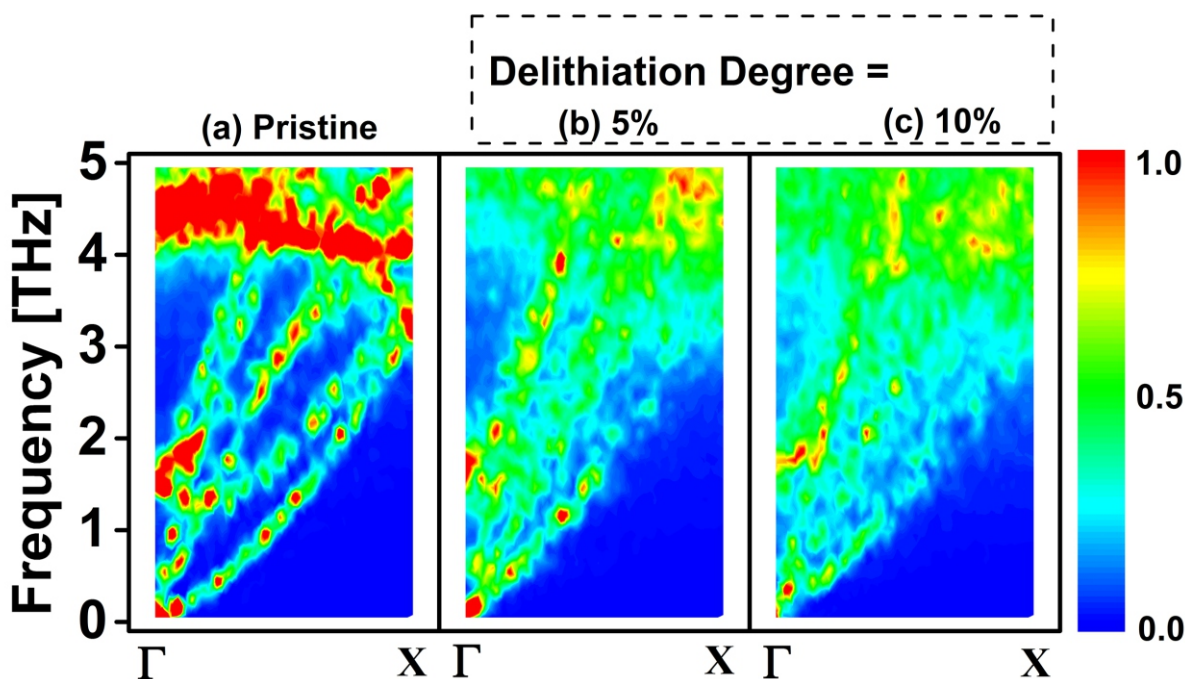
Fig. 5. The spectral energy density of pristine $LiCoO_2$ and delithiation $LiCoO_2$. Spectral energy density of the pristine $LiCoO_2$ (a) and the delithiated $LiCoO_2$ with delithiation degree of 5% (b) and 10% (c), respectively.

TA$_2$) branches are very clear. And a slight broadening of SED curve is observed, which originates from the temperature-dependent anharmonic phonon-phonon interactions.[43] In contrast, a more pronounced broadening of SED curve is observed in the delithiated $LiCoO_2$ (Fig. 5b-c), and the magnitude of SED is substantially reduced compared to that in the pristine $LiCoO_2$. For each phonon mode, the broadening range of SED, which is related to the phonon-defect scattering intensity, directly reflects the phonon relaxation time.[44] The larger broadening in SED indicates a smaller phonon relaxation time. Therefore, the broadening and reduced magnitude of SED curve provide a direct evidence that the phonon relaxation times in delithiated $LiCoO_2$ are reduced compared to the pristine case due to the strong phonon-defect scatterings.[45,46] Moreover, there exists a further broadening and magnitude reduction, revealing a further reduction of the relaxation time, when the delithiation degree changes from 5% to 10%.

In previous works,[47,48] McGaughey *et al.* has demonstrated that the thermal conductivity contributed by short mean free path (MFP) phonons is temperature independent, while the long MFP phonons dominate the temperature dependence behavior. In the delithiated $LiCoO_2$ structure, the long MFP phonons are suppressed due to the strong phonon defect scattering induced by the delithiation. Thus, the relative contribution from the short-MFP phonons to κ_D increases compared with that in the pristine case, which leads to κ_D present a less sensible dependence on temperature. When the delithiation degree increases, the long MFP phonons are further suppressed, and thus the temperature dependence becomes more insensitive correspondingly.

4. Summary

In summary, we have investigated the effect of delithiation on the thermal transport properties of $LiCoO_2$ via molecular dynamics simulations. With the increase of delithiation degree, the thermal conductivity of delithiated $LiCoO_2$ decreases monotonically, and becomes less sensitive to temperature. The calculation results of the spectral heat energy transmission coefficient and the spectral energy distribution together reveal that the delithiation induces the non-propagating heat transport, giving rise to the substantially decreased thermal conductivity in delithiated $LiCoO_2$. Our study provides valuable guidance for the efficient thermal management in the Li-ion battery.

Reference

1. E. P. Roth and D. H. Doughty, *J. Power Sources,* 2004, **128**, 308-318.
2. K. H. Lee, E. H. Song, Y. L. Jin, B. H. Jung and S. L. Hong, *J. Power Sources,* 2004, **132**, 201-205.
3. H. Maleki, G. Deng, A. Anani and J. Howard, *J. Electorchem. Soc.,* 1999, **146**, 3224-3229.
4. J. Cho, M. D. Losego, H. G. Zhang, H. Kim, J. Zuo, I. Petrov, D. G. Cahill and P. V. Braun, *Nat. Commun.,* 2014, **5**, 4035.
5. X. Li and X. Sun, *Recent Progress in Understanding of Lithium Storage Behavior of Graphene Nanosheet Anode for Lithium Ion*

Batteries in the book of *Graphene Science Handbook*, CRC Press, 2014.

6. R. S. Liu, L. Zhang, X. Sun, H. Liu and J. Zhang, *Electrochemical Technologies for Energy Storage and Conversion*, Wiley-VCH, 2012.

7. M. S. Islam and C. A. Fisher, *Chem. Soc. Rev.*, 2014, **43**, 185-204.

8. A. V. D. Ven, J. Bhattacharya and A. A. Belak, *Acc. Chem. Res.*, 2013, **46**, 1216.

9. D. Seo, J. Lee, A. Urban, R. Malik, S. Kang and G. Ceder, *Nat. Chem.*, 2016, **8**, 692-697.

10. D. H. Seo, J. Lee, A. Urban, R. Malik, S. Kang and G. Ceder, *Nat. Chem.*, 2016, **8**, 692-697.

11. R. Malik, F. Zhou and G. Ceder, *Nat. Mater.*, 2011, **10**, 587-590.

12. G. Yoon, D. H. Kim, I. Park, D. Chang, B. Kim, B. Lee, K. Oh and K. Kang, *Adv. Funct. Mater.*, 2017, **27**, 1702887.

13. M. E. A. Y. D. Dompablo, A. V. D. Ven and G. Ceder, *Phys. Rev. B*, 2002, **66**, 064112.

14. Y. S. Meng, Y. W. Wu, J. H. Bing, L. Yi and G. Ceder, *J. Electrochem. Soc.*, 2004, **151**, A1134-A1140.

15. B. J. Hwang, Y. W. Tsai, a. D. Carlier and G. Ceder, *Chem. Mater.*, 2003, **15**, 3676-3682.

16. W. Li, Y. Yang, G. Zhang and Y. W. Zhang, *Nano Lett,* 2015, **15**, 1691-1697.

17. J. Chen, G. Zhang and B. Li. Molecular Dynamics Simulations for Computing Thermal Conductivity of Nanomaterials. (Pan Stanford Publishing, 2015).

18. Z. Zhang, J. Chen and B. Li, *Nanoscale,* 2017, **9**, 14208–14214.

19. Z. Zhang, S. Hu, J. Chen and B. Li, *Nanotechnology,* 2017, **28**, 225704.

20. L. Yang, J. Chen, N. Yang and B. Li, I*nt. J. Heat Mass Transfer,* 2015, **91**, 428-432.

21. S. Plimpton, *J. Comp. Phys.,* 1995, **117**, 1-19.

22. C. AJ Fisher, M. Saiful Islam and H. Moriwake, *J. Phys. Soc. Jpn.,* 2010, **79**, 59-64.

23. N. Yang, G. Zhang and B. Li, *Nano Lett.,* 2008, **8**, 276-280.

24. J. Chen, G. Zhang and B. Li, *J. Phys. Soc. Jpn.,* 2010, **79**, 074604.

25. D. Alexeev, J. Chen, J. H. Walther, K. P. Giapis, P. Angelikopoulos and P. Koumoutsakos, *Nano Lett.,* 2015, **15**, 5744-5749.

26. M. An, Q. Song, X. Yu, H. Meng, D. Ma, R. Li, Z. Jin, B. Huang and N. Yang, *Nano Lett.,* 2017, **17**, 5805-5810.

27. X. Wang and A. Tabarraei, *Appl. Phys. Lett.,* 2016, **108**, 191905.

28. S. Hu, J. Chen, N. Yang and B. Li, *Carbon,* 2017, **116**, 139-144.

29. C. A. Ratsifaritana and P. G. Klemens, *Int. J. Thermophys,* 1987, **8**, 737-750.

30. K. Sääskilahti, J. Oksanen, J. Tulkki and S. Volz, *Phys. Rev. E,* 2016, **93**, 052141.

31. K. Sääskilahti, J. Oksanen, S. Volz and J. Tulkki, *Phys. Rev. B,* 2015, **91**, 115426.

32. K. Q. Chen, W. X. Li, W. Duan, Z. Shuai and B. L. Gu, *Phys. Rev. B,* 2005, **72**, 045422

33. G. Xie, Y. Shen, X. Wei, L. Yang, H. Xiao, J. Zhong and G. Zhang, *Sci. Rep.,* 2014, **4**, 5085.

34. *G. Chen. Nanoscale energy transport and conversion : a parallel treatment of electrons, molecules, phonons, and photons.* (Oxford University Press, 2005).

35. P. B. Allen and J. L. Feldman, *Phys. Rev. B*, 1993, **48**, 12581-12588.

36. T. Zhu and E. Ertekin, *Nano Lett.,* 2016, **16**, 4763-4772.

37. W. Xu, G. Zhang and B. Li, *Appl. Phys. Lett.*, 2015, **116**, 134303.

38. J. M. Larkin and A. J. H. Mcgaughey, *Phys. Rev. B,* 2014, **89**, 144303.

39. T. S. Zhu, K. Swaminathan-Gopalan, K. J. Cruse, K. Stephani and E. Ertekin, *Adv. Funct. Mater.,* 2018, **28**, 1706268.

40. P. B. Allen, J. L. Feldman, J. Fabian and F. Wooten, *Philos Mag B,* 1999, **79**, 1715-1731.

41. S. Hu, M. An, N. Yang and B. Li, *Nanotechnology,* 2016, **27**, 265702.

42. M.Kaviany. *Heat Transfer Physics*, Cambridge University Press, New York, 2008.

43. J. A. Thomas, J. E. Turney, R. M. Iutzi, C. H. Amon and A. J. H. McGaughey, *Phys. Rev. B,* 2010, **81**, 081411.

44. J. Chen, G. Zhang and B. Li, *Nanoscale,* 2013, **5**, 532-536.

45. X. Qian, X. Gu and R. Yang, *Appl. P*hys. Lett.,* 2016, **108**, 6050-6051.

46. Z. Ding, Q. X. Pei, J. W. Jiang and Y. W. Zhang, *J. Phys. Chem.: C,* 2015, **38**, 16358−16365.

47. A. J. H. McGaughey and M. Kaviany, *Int J. Heat Mass Tran,* 2004, **47**, 1799-1816.

48. A. J. H. McGaughey and M. Kaviany, *Int J. Heat Mass Tran,* 2004, **47**, 1783-1798.